

## Chapter

## 1

# THE CHARACTERISTICS OF SUNLIGHT

## 1.1 PARTICLE-WAVE DUALITY

Our understanding of the nature of light has changed back and forth over the past few centuries between two apparently conflicting viewpoints. A highly readable account of the evolution of quantum theory is given in Gribben (1984). In the late 1600s, Newton's mechanistic view of light as being made up of small particles prevailed. By the early 1800s, experiments by both Young and Fresnel had shown interference effects in light beams, indicating that light was made up of waves. By the 1860s, Maxwell's theories of electromagnetic radiation were accepted, and light was understood to be part of a wide spectrum of electromagnetic waves with different wavelengths. In 1905, Einstein explained the photoelectric effect by proposing that light is made up of discrete particles or *quanta* of energy. This complementary nature of light is now well accepted. It is referred to as the particle-wave duality, and is summarised by the equation

$$E = hf = hc / \lambda \quad (1.1)$$

where light, of frequency  $f$  or wavelength  $\lambda$ , comes in 'packets' or *photons*, of energy  $E$ ,  $h$  is Planck's constant ( $6.626 \times 10^{-34}$  Js) and  $c$  is the velocity of light ( $3.00 \times 10^8$  m/s) (NIST, 2002).

In defining the characteristics of photovoltaic or 'solar' cells, light is sometimes treated as waves, other times as particles or photons.

## 1.2 BLACKBODY RADIATION

A ‘blackbody’ is an ideal absorber, and emitter, of radiation. As it is heated, it starts to glow; that is, to emit electromagnetic radiation. A common example is when a metal is heated. The hotter it gets, the shorter the wavelength of light emitted and an initial red glow gradually turns white.

Classical physics was unable to describe the wavelength distribution of light emitted from such a heated object. However, in 1900, Max Planck derived a mathematical expression describing this distribution, although the underlying physics was not understood until Einstein’s work on ‘quanta’ five years later. The spectral emissive power of a blackbody is the power emitted per unit area in the wavelength range  $\lambda$  to  $\lambda + d\lambda$  and is given by the Planck distribution (Incropera & DeWitt, 2002),

$$E(\lambda, T) = \frac{2\pi hc^2}{\lambda^5 [\exp(hc/(\lambda kT)) - 1]} \quad (1.2)$$

where  $k$  is Boltzmann’s constant and  $E$  has dimensions of power per unit area per unit wavelength. The total emissive power, expressed in power per unit area, may be found by integration of Eqn. (1.2) over all possible wavelengths from zero to infinity, yielding  $E = \sigma T^4$ , where  $\sigma$  is the Stefan-Boltzmann constant (Incropera & DeWitt, 2002).

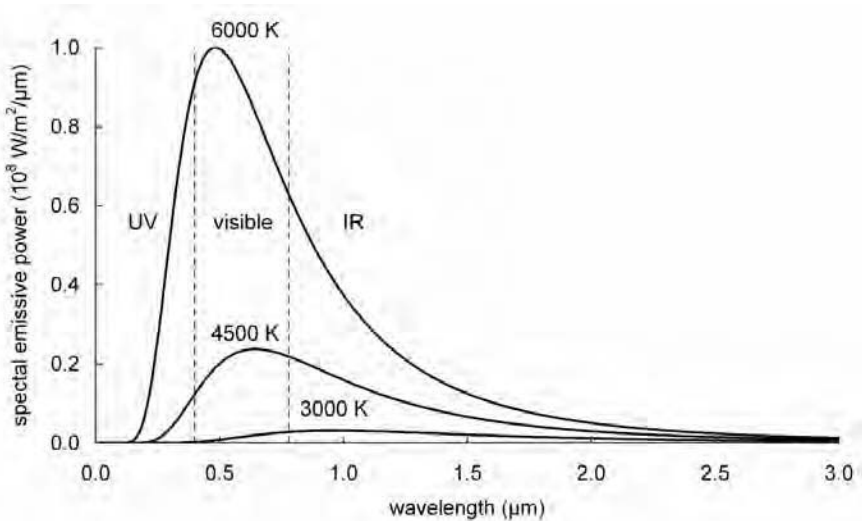


Figure 1.1. Radiation distributions from perfect blackbodies at three different temperatures, as would be observed at the surface of the blackbodies.

Fig. 1.1 illustrates the radiation distribution for different blackbody temperatures, as would be observed at the surface of the blackbody. The lowermost curve is that for a body heated to 3000 K, about the temperature of the tungsten filament in an incandescent lamp. The wavelength of peak energy emission is about 1  $\mu\text{m}$ , in the infrared. Only a small amount of energy is emitted at visible wavelengths (0.4–0.8  $\mu\text{m}$ ) in this case, which explains why these lamps are so inefficient. Much higher

temperatures, beyond the melting points of most metals, are required to shift the peak emission to this range.

### 1.3 THE SUN AND ITS RADIATION

The sun is a hot sphere of gas heated by nuclear fusion reactions at its centre (Quaschnig, 2003). Internal temperatures reach a very warm 20 million K. As indicated in Fig. 1.2, the intense radiation from the interior is absorbed by a layer of hydrogen ions closer to the sun's surface. Energy is transferred by convection through this optical barrier and then re-radiated from the outer surface of the sun, the *photosphere*. This emits radiation approximating that from a blackbody with a temperature of nearly 6000 K, as shown in Fig. 1.3.

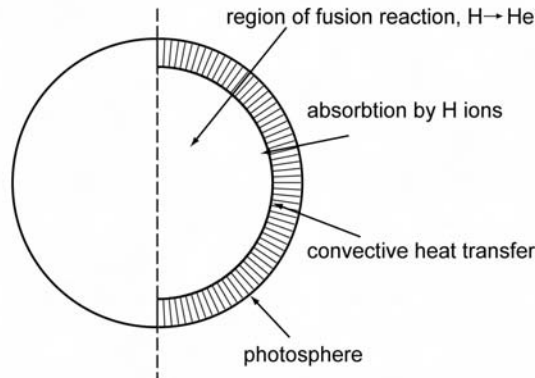


Figure 1.2. Regions in the sun's interior.

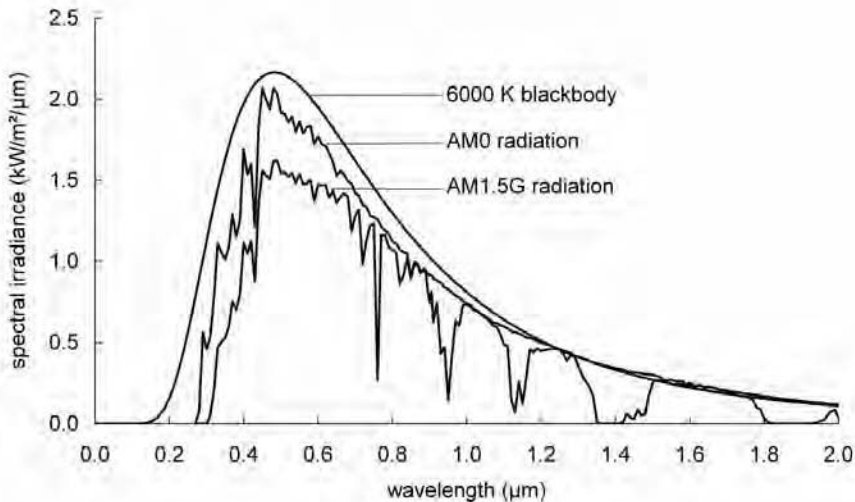


Figure 1.3. The spectral irradiance from a blackbody at 6000 K (at the same apparent diameter as the sun when viewed from earth); from the sun's photosphere as observed just outside earth's atmosphere (AM0); and from the sun's photosphere after having passed through 1.5 times the thickness of earth's atmosphere (AM1.5G).

## 1.4 SOLAR RADIATION

Although radiation from the sun's surface is reasonably constant (Gueymard, 2004; Willson & Hudson, 1988), by the time it reaches the earth's surface it is highly variable owing to absorption and scattering in the earth's atmosphere.

When skies are clear, the maximum radiation strikes the earth's surface when the sun is directly overhead, and sunlight has the shortest pathlength through the atmosphere. This pathlength can be approximated by  $1/\cos\phi$ , where  $\phi$  is the angle between the sun and the point directly overhead, as shown in Fig. 1.4. This pathlength is usually referred to as the *Air Mass* (AM) through which solar radiation must pass to reach the earth's surface. Therefore

$$AM = 1/\cos\phi \quad (1.3)$$

This is based on the assumption of a homogeneous, non-refractive atmosphere, which introduces an error of approximately 10% close to the horizon. Iqbal (1983) gives more accurate formulae that take account of the curved path of light through atmosphere where density varies with depth.

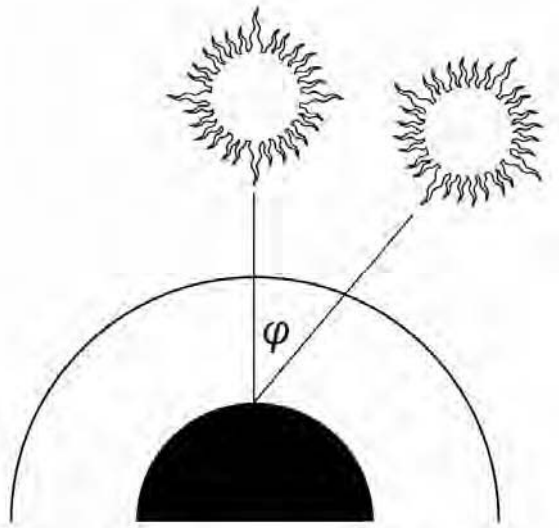


Figure 1.4. The amount of atmosphere (air mass) through which radiation from the sun must pass to reach the earth's surface depends on the sun's position.

When  $\phi = 0$ , the Air Mass equals 1 or 'AM1' radiation is being received; when  $\phi = 60^\circ$ , the Air Mass equals 2 or 'AM2' conditions prevail. AM1.5 (equivalent to a sun angle of  $48.2^\circ$  from overhead) has become the standard for photovoltaic work.

The Air Mass (AM) can be estimated at any location using the following formula:

$$AM = \sqrt{1 + (s/h)^2} \quad (1.4)$$

where  $s$  is the length of the shadow cast by a vertical post of height  $h$ , as shown in Fig. 1.5.

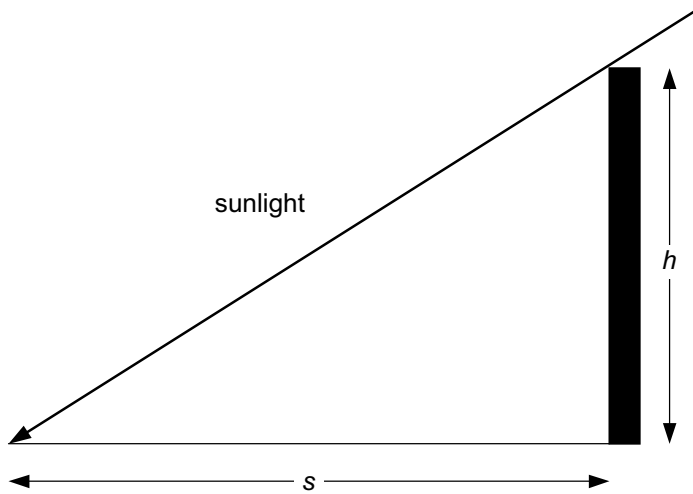


Figure 1.5. Calculation of Air Mass using the shadow of an object of known height.

The spectral distribution of sunlight outside the atmosphere (*Air Mass Zero* or AM0), and at AM1.5 are shown in Fig. 1.6. Air Mass Zero is essentially unvarying and its total power density, integrated over the spectrum, is referred to as the *solar constant*, with a generally accepted value (ASTM, 2000, 2003; Gueymard, 2004) of

$$\gamma = 1.3661 \text{ kW/m}^2 \quad (1.5)$$

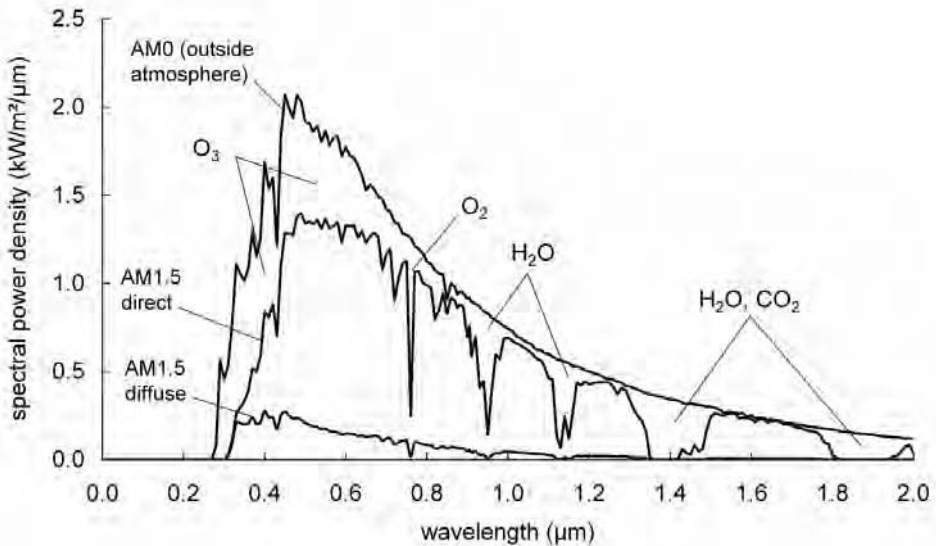


Figure 1.6. The spectral power density of sunlight, outside the atmosphere (AM0) and at the earth's surface (AM1.5), showing absorption from various atmospheric components.

It is common to consider separately the ‘direct’ (or ‘beam’) radiation from the solar disk and the ‘diffuse’ radiation from elsewhere in the sky, with their sum known as ‘global’ radiation. A table of AM1.5 global (AM1.5G) irradiance versus wavelength for an equator-facing, 37° tilted surface on earth is given in Appendix A. Since different types of photovoltaic cells respond differently to different wavelengths of light, the tables can be used to assess the likely output of different cells.

For the spectrum of Appendix A, the total energy density, i.e. the integral of the power density over the entire wavelength band, is close to 970 W/m<sup>2</sup>. This spectrum, or the corresponding ‘normalised’ spectrum of 1000 W/m<sup>2</sup>, is the present standard used for rating photovoltaic products. The latter is close to the maximum power received at the earth’s surface. The power and photon flux density components corresponding to the ‘normalised’ spectrum can be obtained by multiplying the Appendix A values by 1000/970.

To assess the likely performance of a photovoltaic cell or module in a real system, the standard spectra discussed above must be related to the actual solar insolation levels for the site at which the system is to be installed. (Fig. 1.12 illustrates the global and seasonal variation in daily insolation levels.)

## 1.5 DIRECT AND DIFFUSE RADIATION

Sunlight passing through the earth’s atmosphere is attenuated, or reduced, by about 30% by the time it reaches the earth’s surface due to such effects as (Gast, 1960; Iqbal, 1983):

1. Rayleigh scattering by molecules in the atmosphere, particularly at short wavelengths ( $\sim\lambda^{-4}$  dependence)
2. Scattering by aerosols and dust particles.
3. Absorption by atmospheric gases such as oxygen, ozone, water vapour and carbon dioxide (CO<sub>2</sub>).

The latter produces the absorption bands apparent in Fig. 1.3. Wavelengths below 0.3 μm are strongly absorbed by ozone. Depletion of ozone from the atmosphere allows more of this short wavelength light to reach the earth, with consequent harmful effects on biological systems. The absorption bands around 1 μm are produced by water vapour absorption, complemented by CO<sub>2</sub> absorption at longer wavelengths. Changing the CO<sub>2</sub> content of the atmosphere also has consequences for the earth’s climatic and biological systems.

Fig. 1.7 shows how atmospheric scattering results in a diffuse component of sunlight coming from all directions in the sky. Diffuse radiation is predominantly at the blue end of the spectrum because of more effective scattering at small wavelengths. Hence, the sky appears blue.

AM1 radiation (radiation when the sun is directly overhead), has a diffuse component of about 10% when skies are clear. The percentage increases with increasing air mass or when skies are not clear.

Cloud cover is, of course, a significant cause of radiation attenuation and scattering. *Cumulus* or bulky, low altitude clouds, are very effective in blocking sunlight.

However, about half the direct beam radiation blocked by cumulus clouds is recovered in the form of diffuse radiation. *Cirrus*, or wispy, high altitude clouds, are not as effective in blocking sunlight, and about two thirds of the direct beam radiation blocked is converted to diffuse radiation. On a totally cloudy day, with no sunshine, most radiation reaching the earth's surface will be diffuse (Liu & Jordan, 1960).

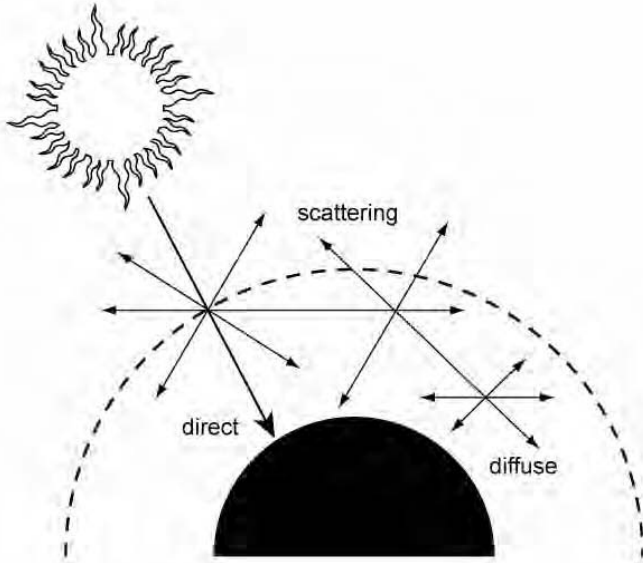


Figure 1.7. Atmospheric scattering leading to diffuse radiation.

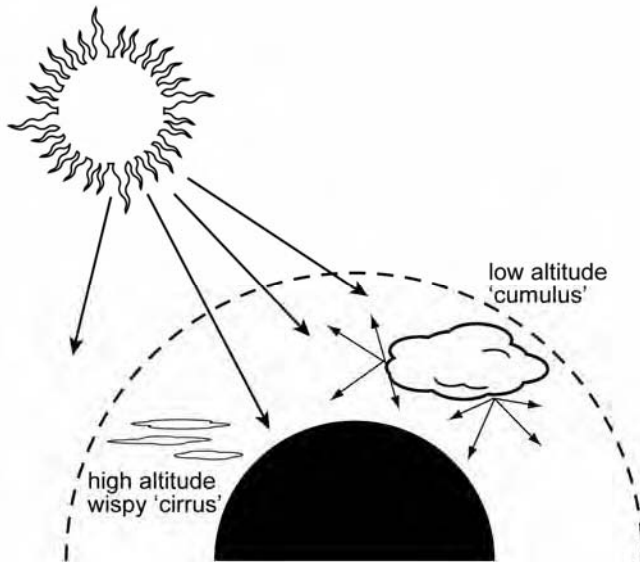


Figure 1.8. The effect of cloud cover on radiation reaching the earth's surface.

## 1.6 THE GREENHOUSE EFFECT

To maintain the earth's temperature, energy reaching the earth from the sun must equal energy radiated back out from the earth. As with incoming radiation, the atmosphere interferes with outgoing radiation. Water vapour absorbs strongly in the 4–7  $\mu\text{m}$  wavelength band and carbon dioxide in the 13–19  $\mu\text{m}$  wavelength band. Most outgoing radiation (70%) escapes in the 'window' between 7 and 13  $\mu\text{m}$ .

If we had no atmosphere, as on the moon, the average temperature on the earth's surface would be about  $-18^\circ\text{C}$ . However, a natural background level of 270 ppm  $\text{CO}_2$  in the atmosphere causes the earth's temperature to be about  $15^\circ\text{C}$  on average,  $33^\circ\text{C}$  greater than the moon's. Fig. 1.9 shows the wavelength distribution of incoming and outgoing energy if the earth and the sun were ideal blackbodies.

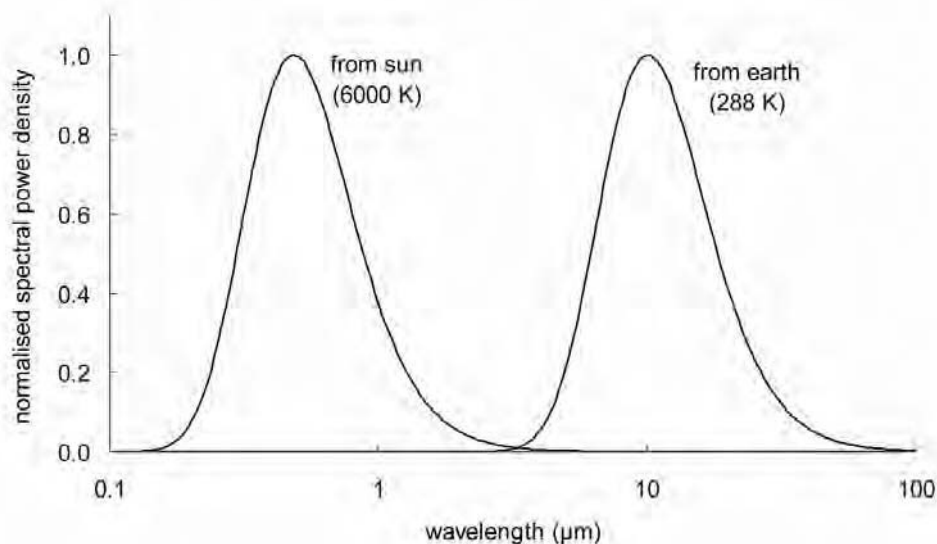


Figure 1.9. Spectral distribution of incoming and outgoing radiation at the earth's surface if both earth and sun are treated as black bodies. (Note that the peaks of the two curves have been normalised and the scale of the horizontal axis is logarithmic.)

Human activities are increasingly releasing 'anthropogenic gases' into the atmosphere, which absorb in the 7–13  $\mu\text{m}$  wavelength range, particularly carbon dioxide, methane, ozone, nitrous oxides and chlorofluorocarbons (CFCs). These gases are preventing the normal escape of energy and are widely accepted to be causing observed increases in average terrestrial temperatures. According to McCarthy *et al.* (2001), 'Globally-averaged surface temperatures have increased by  $0.6 \pm 0.2^\circ\text{C}$  over the 20th century, and the globally-averaged surface air temperature is projected by models to warm  $1.4\text{--}5.8^\circ\text{C}$  above 1990 levels by 2100. These projections indicate that the warming would vary by region, and be accompanied by increases and decreases in precipitation. In addition, there would be changes in the variability of climate, and changes in the frequency and intensity of some extreme climate phenomena.' There are already indications of increased floods and droughts, and a wide range of serious impacts on human and natural systems are predicted.

Clearly, human activities have now reached a scale where they are impacting on the planet's self-support systems. The side-effects could be devastating and technologies with low environmental impact and low 'greenhouse gas' emissions will increase in importance over the coming decades. Since the energy sector is the major producer of greenhouse gases via the combustion of fossil fuels, technologies such as photovoltaics, which can be substituted for fossil fuels, should increasingly be used (Blakers *et al.*, 1991).

### 1.7 APPARENT MOTION OF THE SUN

The apparent motion of the sun (Iqbal, 1983; Sproul, 2002), and its position at solar noon, relative to a fixed observer at latitude  $35^{\circ}\text{S}$  (or N) is shown in Fig. 1.10. The sun's path varies over the year and is shown at its extreme excursions, the summer and winter solstices, as well as at the equinoxes, its mid-season position. At the equinoxes, (around March 21 and September 23), the sun rises due east and sets due west and at solar noon, the altitude equals  $90^{\circ}$  minus the latitude. At the winter and summer solstices (around June 21 and December 22, respectively, for the southern hemisphere and the opposite for the northern hemisphere), the altitude at solar noon is increased or decreased by the inclination of the earth's axis ( $23^{\circ}27'$ ). Equations that allow the sun's position in the sky to be calculated at any point in time are given in Appendix B. The apparent solar trajectory is sometimes indicated in the form of polar (Fig. 1.11) or cylindrical diagrams. The latter are particularly useful for overlaying the shading effects of nearby objects (Duffie & Beckman, 1991; Quaschnig & Hanitsch, 1995; Skiba *et al.*, 2000). An online calculator for cylindrical sun charts is available from the University of Oregon Solar Radiation Monitoring Laboratory (University of Oregon, 2003).

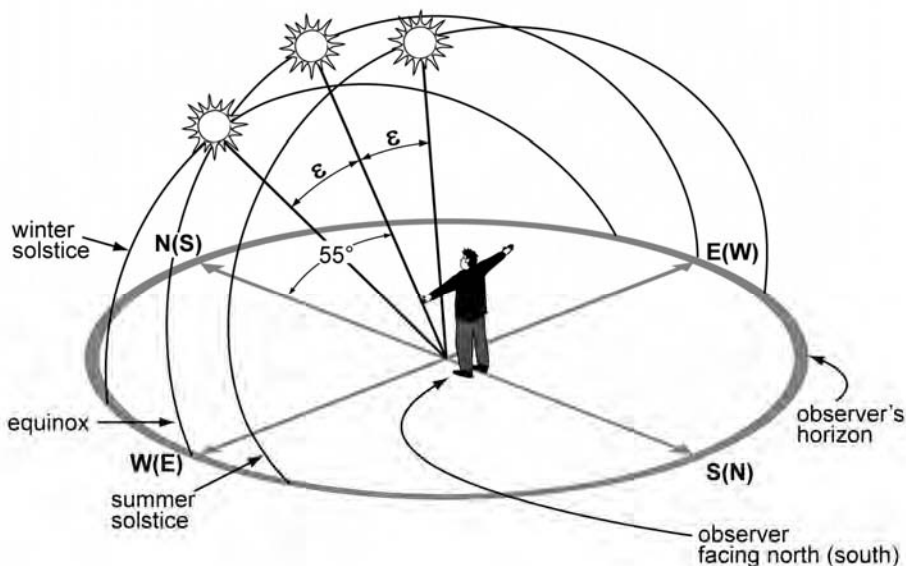


Figure 1.10. Apparent motion of the sun for an observer at  $35^{\circ}\text{S}$  (or N), where  $\epsilon$  is the inclination of the earth's axis of rotation relative to its plane of revolution about the sun ( $= 23^{\circ}27' = 23.45^{\circ}$ ).

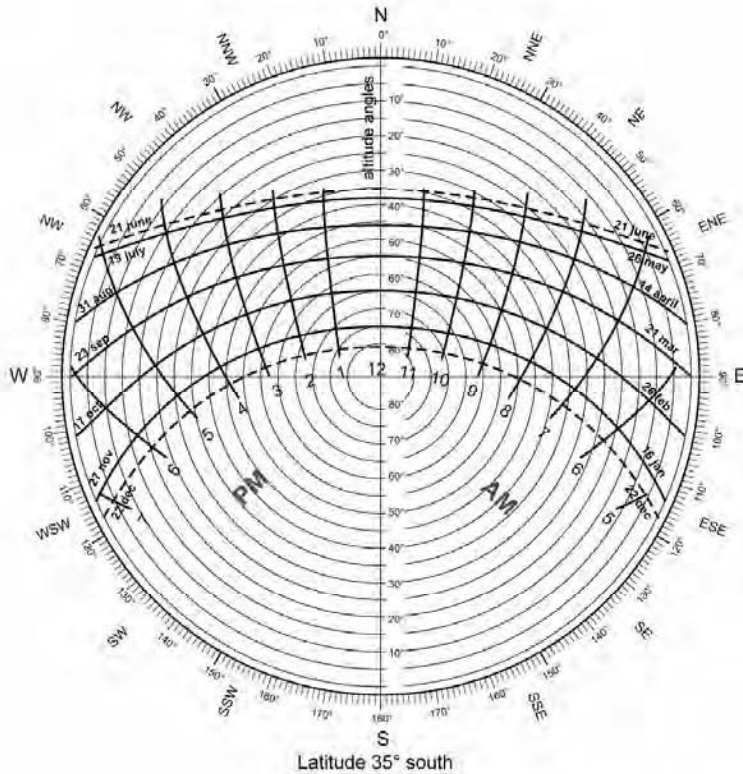


Figure 1.11. Polar chart showing the apparent motion of the sun for an observer at 35°S. ("Copyright © CSIRO 1992, Reproduced by permission of CSIRO PUBLISHING, Melbourne Australia from *Sunshine and Shade in Australasia* 6th edition (R.O. Phillips) <http://www.publish.csiro.au/pid/147.htm>)

### 1.8 SOLAR INSOLATION DATA AND ESTIMATION

Good reviews of this field have been done by, for example, Duffie and Beckman (1991), Iqbal (1983), Reddy (1987), Perez *et al.* (2001) and Lorenzo (1989, 2003). Extraterrestrial irradiation is known from geometry and the solar constant (see Eqn. 1.5) but terrestrial intensities are less well defined.

Photovoltaic system designers often need estimates of the insolation expected to fall on arbitrarily-tilted surfaces. For most purposes, monthly average daily insolation values are sufficient (Lorenzo, 2003) and 'characteristic' days near the middle of each month are often used to define average monthly values (Appendix C). Asterisks are used in this book to denote variables based on characteristic days and overbars indicate monthly averages. Separated direct and diffuse components are usually required for estimation of the effects of module tilt, but these need to be estimated from global values if not separately measured. Hence, there are three basic problems:

1. Evaluating the global radiation on a horizontal surface for a given site from available measured quantities.

2. Evaluating the horizontal direct and diffuse components from the global values.
3. Estimating these components for a tilted plane from the horizontal values.

### 1.8.1 Extraterrestrial radiation

$R_0$ , the extraterrestrial radiation on a horizontal surface, may be calculated from  $\gamma_E$ , the solar constant expressed as energy incident in one hour

$$\gamma_E = 3.6\gamma \quad (\text{kJm}^{-2}\text{h}^{-1}) \quad (1.6)$$

and the geometry of the sun and earth (Iqbal, 1983, p. 65)

$$R_0 = \left(\frac{24}{\pi}\right) \gamma_E e_0 \cos \varphi \cos \delta \left[ \sin \omega_s - \left(\frac{\pi \omega_s}{180}\right) \cos \omega_s \right] \quad (1.7)$$

where

$$e_0 \approx 1 + 0.033 \cos\left(\frac{2\pi d}{365}\right) \quad (1.8)$$

is the orbital eccentricity (the reciprocal of the square of the radius vector of the earth) (Iqbal, 1983) (a more accurate expression for the eccentricity is also available in Lorenzo, 1989),  $\omega_s$  is the sunrise hour angle, defined by

$$\cos \omega_s = \tan \varphi \tan \delta \quad (1.9)$$

$d$  is the day number starting with 1 January as  $d = 1$  (February is always assumed to have 28 days, introducing a small error in leap years), and  $\delta$  is the declination of the sun as given by

$$\delta \approx \sin^{-1} \left\{ \sin \varepsilon \cdot \sin \left[ \frac{(d-81)360}{365} \right] \right\} \approx \varepsilon \sin \left[ \frac{(d-81)360}{365} \right] \quad (1.10)$$

where  $\varepsilon = 23.45^\circ$ . The declination is the angle between a line joining the earth and sun centres and the earth's equatorial plane and is zero at the equinoxes (Iqbal, 1983). More complicated and accurate expressions are also available (see Appendix B).

The corresponding monthly average of extraterrestrial daily global radiation on a horizontal surface is given by

$$\bar{R}_0 = \left(\frac{24}{\pi}\right) \gamma_E e_0^* \cos \varphi \cos \delta^* \left[ \sin \omega_s^* - \left(\frac{\pi \omega_s^*}{180}\right) \cos \omega_s^* \right] \quad (1.11)$$

### 1.8.2 Terrestrial global radiation on a horizontal surface

Various instruments exist for measuring insolation levels (Iqbal, 1983; Tindell & Weir, 1986). The simplest is a heliograph, which measures the hours of bright sunshine by using focussed light to burn a hole in a rotating chart. Silicon solar cells themselves are used in the next most sophisticated group of equipment. The

thermoelectric effect (voltage generated by heat differences across junctions of dissimilar material) forms the basis of the more accurate equipment (pyrometers, pyrliometers) since this effect is less sensitive to the wavelength of light.

Obtaining accurate solar insolation data in an appropriate form is obviously important for designing photovoltaic systems but it is sometimes a difficult task. One of the most widely available data forms is the average daily, monthly, quarterly or annual total global (direct and diffuse) radiation falling on a horizontal or tilted surface. Examples are shown in Fig. 1.12, which gives the quarterly-average global isoflux contours for each quarter in MJ/m<sup>2</sup> per day. Similar global plots are available from Sandia National Laboratories (1991). Where possible, more exact data for each particular location should be sought, preferably in the form of direct and diffuse components rather than global insolation levels. Some sources of insolation data are listed in Appendix D. Direct and diffuse components have been measured and are available for some locations. Data for several Australian sites have been processed into a range of forms useful to solar energy engineers and architects (Lee *et al.*, 2003).

### **Peak sun hours data**

Average daily insolation values for each month are sometimes presented in the form of ‘peak sun hours’. Conceptually, the energy received throughout the day, increasing from low intensity in the morning, peaking at solar noon and declining during the afternoon, is compressed into a reduced duration of noon intensity sunlight (Sandia National Laboratories, 1991). If the intensity of noon insolation (peak sun) is approximated to 1.0 kW/m<sup>2</sup>, the number of peak sun hours coincides with the total daily insolation measured in kWh/m<sup>2</sup>.

### **Sunshine hours data**

A form in which solar insolation data are commonly available is as ‘sunshine hours’ (SSH) (Twidell & Weir, 2006). This term indicates the number of daily hours of sunlight above a certain intensity, approximately 210 W/m<sup>2</sup>, for a given period (usually a month), but gives no indication of absolute values and applies only to the direct component of sunlight. The measurements of ‘sunshine hours’ are made on a Campbell-Stokes sunshine hours instrument by concentrating parallel rays of light onto a small area of moving tape, which burns if the sun is shining brightly. Diffuse light cannot be concentrated in the same way and is not recorded by the instrument. The resulting data are not very high quality and are not recommended for use except where they can be reliably correlated with irradiation (Standards Australia, 2002), but are available for many locations where irradiation has not been recorded.

For PV system design, the difficulty is in converting SSH data to a useable form. Here we consider techniques for estimating, from SSH data, the monthly average of daily global radiation incident on a horizontal surface (Iqbal 1983)

$$\bar{R} = \bar{R}_o(a + b \bar{n} / \bar{N}_d) \quad (1.12)$$

where  $\bar{R}_o$  is defined by Eqn. (1.11),  $\bar{n}$  is the recorded monthly average of bright sunshine hours per day, as measured by a Campbell-Stokes instrument,  $a$  and  $b$  are

regression ‘constants’ extracted from measured data at various locations, and  $\bar{N}_d$  is the monthly average day length =  $2/15\omega_s^*$ .

This model was used by Telecom (now Telstra) Australia (Muirhead & Kuhn, 1990), who determined  $a$  and  $b$  values as listed in Table 1.1 and ‘averages’ for Australia of

$$a = 0.24 \text{ and } b = 0.48, \quad (1.13)$$

although some dependence on latitude was found.

See Appendix D for some sources of extracted  $a$  and  $b$  values for various world locations. Extensive records are available for many sites across Australia as well as some isolated islands and Antarctica.

Table 1.1. Regression data for Australian sites (Muirhead & Kuhn, 1990).

Site	Latitude °	$a$	$b$
Adelaide	34.9	0.24	0.51
Alice Springs	23.8	0.24	0.51
Brisbane	27.5	0.23	0.46
Darwin	12.5	0.28	0.46
Hobart	42.8	0.23	0.47
Laverton	37.9	0.24	0.49
Mt. Gambier	37.8	0.26	0.46
Perth	32.0	0.22	0.49
Sydney	33.9	0.23	0.48
Wagga Wagga	35.2	0.27	0.52

More complicated expressions (Reitveld, 1978)

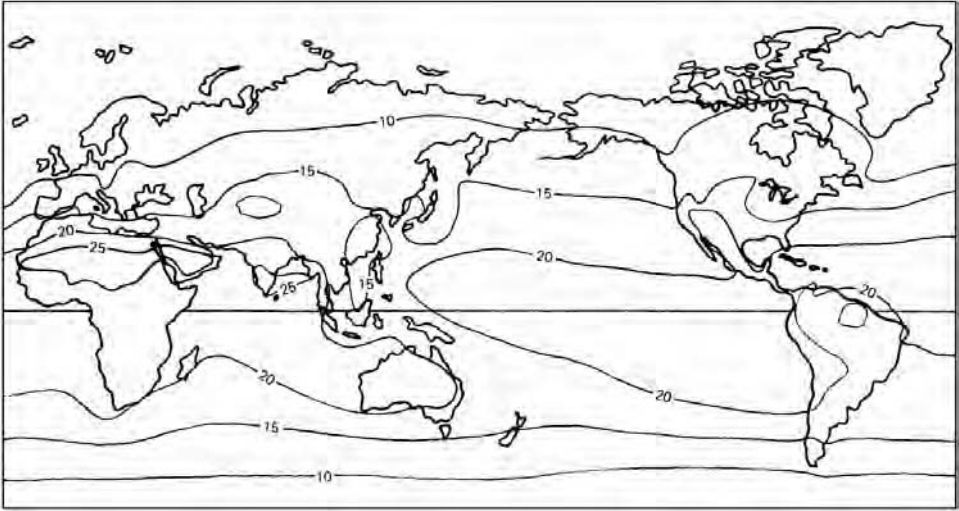
$$a = 0.10 + 0.24 \bar{n}/\bar{N}_d \text{ and } b = 0.38 + 0.08 \bar{n}/\bar{N}_d \quad (1.14)$$

have been determined through the use of data generated from sites all around the world. This is supposed to be applicable globally and to be superior to other correlations for cloudy conditions (Iqbal, 1983). Latitude dependence (for latitude  $\theta < 60^\circ$ ) has been introduced by Glover and McCulloch (1958), giving

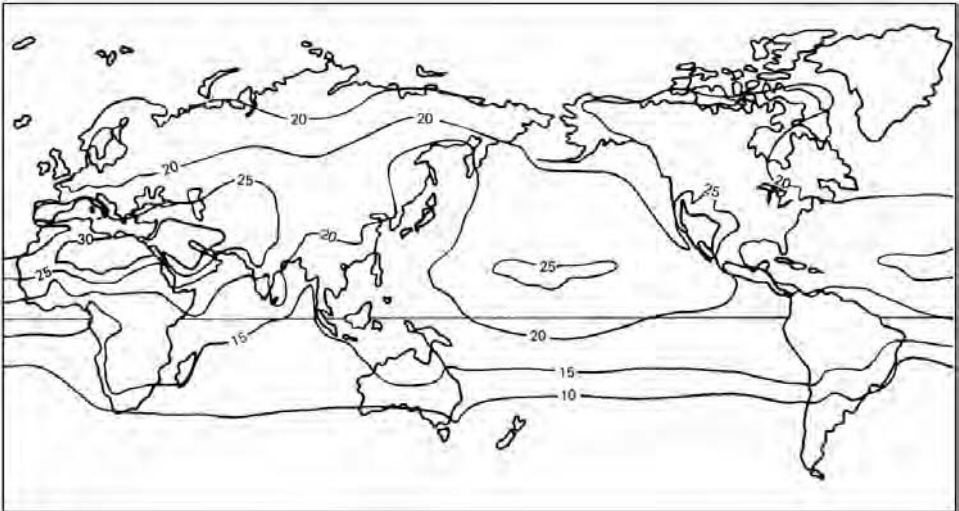
$$\bar{R} = \bar{R}_o [0.29 \cos \theta + 0.52 (\bar{n}/\bar{N}_d)] \quad (1.15)$$

There are reasons for caution in using  $a$  and  $b$  values from the literature. Various values for geometric and insolation parameters have been used in their derivation, measured data have come from a variety of instruments using a variety of methods, and data obtained in different ways have sometimes been mixed and treated as if of identical form (Iqbal, 1983).

Another way of estimating global radiation from SSH data is to use the value of  $\bar{n}/\bar{N}_d$  as an estimate of the percentage of ‘sunny days’, with  $(\bar{N}_d - \bar{n})/\bar{N}_d$  being the corresponding percentage of ‘cloudy days’. The air mass values throughout each day for the given latitude and time of year are then used to estimate quite accurately the direct component of insolation via Eqn. (1.20) below. The diffuse component can then be estimated by assuming that 10% of the insolation on a ‘sunny day’ is diffuse and that the average solar intensity on a ‘cloudy day’ is 20% that of a ‘sunny day’.

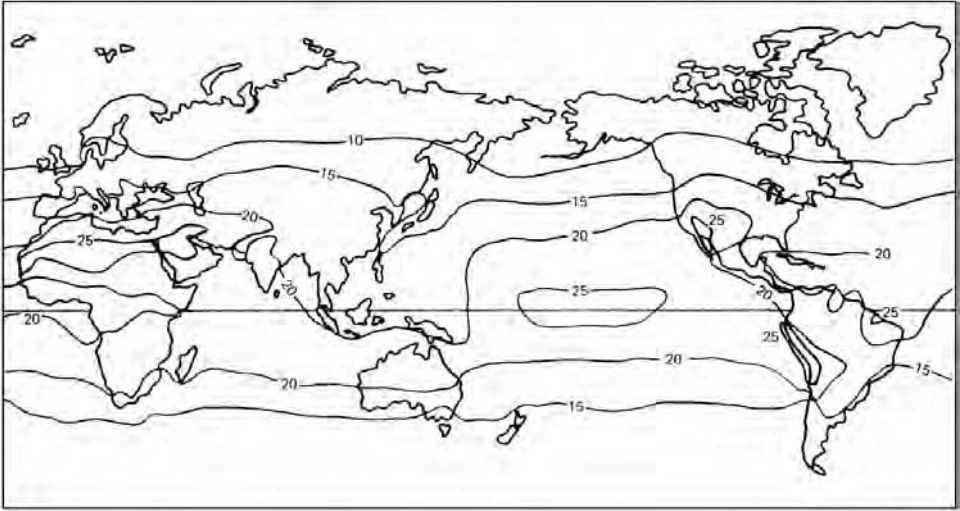


a

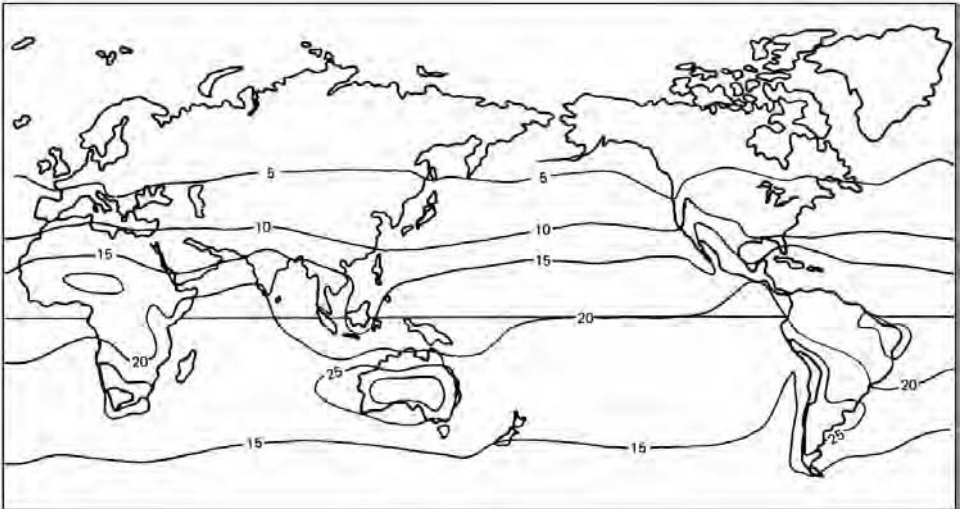


b

Figure 1.12. Average quarterly global isoflux contours of total insolation per day in  $\text{MJ/m}^2$  falling on a horizontal surface ( $1 \text{ MJ/m}^2 = 0.278 \text{ kWh/m}^2$ ). (a) March quarter, (b) June quarter (Used with permission of the authors, Meinel & Meinel, 1976).



c



d

Figure 1.12 (continued). Average quarterly global isoflux contours of total insolation per day in  $\text{MJ}/\text{m}^2$  falling on a horizontal surface ( $1 \text{ MJ}/\text{m}^2 = 0.278 \text{ kWh}/\text{m}^2$ ). (c) September quarter, (d) December quarter (Used with permission of the authors, Meinel & Meinel, 1976).

### **Typical meteorological year (TMY) data**

Insolation data is sometimes available in the form of a ‘typical meteorological year’ (TMY) data set (Hall, 1978; Perez, 2001; Lorenzo, 2003). This is a full year of data combined from individual months, each of which has been selected from an historical record as being ‘typical’. Several selection methods exist and smoothing may be applied to reduce discontinuities that could arise from concatenating months of data from different years (Perez, 2001). Lorenzo (2003) argues at length that although a TMY data set may consist of hourly values, its use in modelling does not necessarily produce results more accurate than those of a set of 12 monthly values.

### **Satellite cloud cover data**

Every hour, satellite cloud cover data are updated at the Australian Bureau of Meteorology (2004). The digitised data corresponding to photographs such as that in Fig. 1.13 are also available and have a resolution of 2.5 km. Such data can be fed directly into a computer for processing and analysis to facilitate very accurate estimates of percentages of cloudy and sunny weather (Beyer *et al.*, 1992). Satellite data, accumulated over many years, can then be used in conjunction with Eqn. (1.19) below, and the equations of Appendix B, to estimate insolation levels.

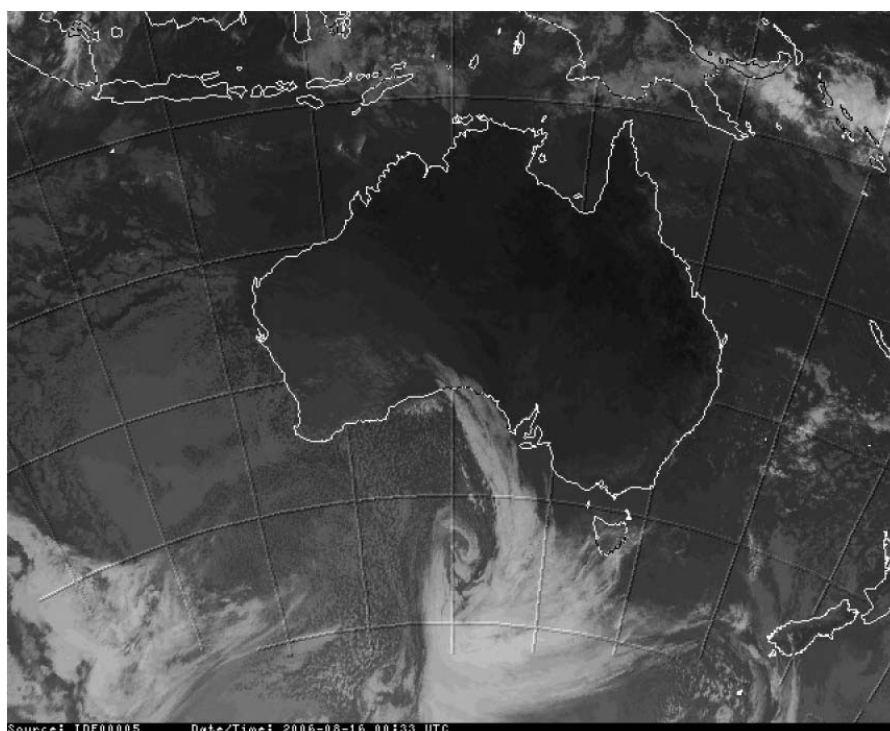


Figure 1.13. Infrared satellite cloud cover photograph, 16 August 2006 (Used with permission of the Bureau of Meteorology, "MTSAT-1R : Satellite image originally processed by the Bureau of Meteorology from the geostationary satellite MTSAT-1R operated by the Japan Meteorological Agency.")

A cloudiness index, corresponding to the fraction of sky blocked by clouds, has been correlated with global radiation (Lorenzo, 1989) and cloud cover (sky cover) data, and is discussed by Iqbal (1983), who considers this form of data to be less reliable than sunshine hour correlations.

Also available for some locations are nephanalysis charts, which portray cloud data by standardised symbols and conventions, showing cloud types, amounts and sizes, the spaces between them and various types of cloud lines and bands. The degrees of coverage are determined by ground-level observations, in conjunction with the satellite picture. Cloud types are usually identified on nephanalyses as stratiform, cumuliform, cirriform and cumulonimbus, with each type able to be characterised in terms of its effects on incident insolation.

### **Satellite-derived insolation estimates**

NASA (2004a) makes freely available satellite-derived estimates of global insolation for the world, on a grid of cells, each 1° latitude × 1° longitude. The data are considered to be the average over the area of the cell. The data are not intended to replace ground measurement data but to fill gaps where ground measurements are missing and to complement ground measurements in other areas. The data quality may at least be accurate enough for preliminary feasibility studies.

Various models are applied to estimate diffuse and direct components and global radiation on tilted surfaces, with the applied methods being documented clearly (NASA, 2004b).

### **1.8.3 Global and diffuse components**

Diffuse insolation is produced by complex interactions with the atmosphere, which absorbs and scatters, and the earth's surface, which absorbs and reflects.

Measurements of diffuse insolation, which require pyranometers fitted with shadow bands to block direct sunlight, are available for far fewer sites than are measurements of global insolation. Hence, methods have been developed to estimate the diffuse fraction from the global value.

### **Clearness index**

Liu and Jordan (1960) estimated the diffuse fraction of sunlight from the monthly average clearness index,  $\bar{K}_T$ , defined by:

$$\bar{K}_T = \bar{R} / \bar{R}_o \quad (1.16)$$

the ratio of monthly averages of daily diffuse and extraterrestrial global radiation.

The procedure to estimate  $\bar{R}_d$ , the monthly average daily diffuse radiation on a horizontal surface, from published or measured values of  $\bar{R}$  is simply:

1. Calculate  $\bar{R}_o$  for each month using Eqn. (1.7), then

$$\bar{K}_d = \bar{R}_d / \bar{R}_o \quad (1.17)$$

where  $\bar{R}_d$  is the desired result. The latter expression yields the diffuse

component,  $\bar{R}_d$ , from the more commonly measured  $\bar{R}$  if  $\bar{K}_d$  and  $\bar{K}_T$  can be correlated. There are several such correlations in the literature, with that due to Page (1961) being considered the most reliable for latitudes less than 40° (Lorenzo, 2003)

$$\bar{K}_d = 1 - 1.13\bar{K}_T \quad (1.18)$$

2. Estimate  $\bar{K}_T$  for each month using Eqn. (1.16).
3. Estimate  $\bar{K}_d$  for each month using Eqn. (1.18).
4. Estimate  $\bar{R}_d$  for each month using Eqn. (1.17).

Correlation models, such as that of Eqn. (1.18) are available in the literature for different averaging times from one month down to less than one hour. These models depend strongly on the averaging times and should not be applied for different averaging periods (Perez *et al.*, 2001).

### **Telecom model**

If the separate components for diffuse and direct insolation are not known, a reasonable approximation for both (for most locations) may be obtained by equating the total monthly global insolation with the total insolation theoretically calculated for an appropriate number of ‘sunny’ and ‘cloudy’ days. The calculations proceed as follows:

1. **‘Sunny’ days**—The intensity of the direct component of the sunlight throughout each day can be determined as a function of the air mass from the experimentally-based equation (Meinel & Meinel, 1976)

$$I = 1.3661 \times 0.7^{(AM)^{0.678}} \text{ kW/m}^2 \quad (1.19)$$

where the currently accepted value of the solar constant has been inserted in place of the original value,  $I$  is the intensity of the direct component incident on a plane perpendicular to the sun’s rays and air mass ( $AM$ ) values are a function of the latitude, the time of year and the time of day, which can be calculated using the algorithms in Appendix B.

By determining  $I$  values throughout a typical day, the daily direct insolation can be calculated. This value is then increased by 10% to account for the diffuse component, the origin of which is indicated in Fig. 1.14. This then gives the expected daily insolation on a sunny day for the given location and time of year.

2. **‘Cloudy’ days**—All incident light is assumed to be diffuse, with an intensity on a horizontal surface typically 20% of that determined by Eqn. (1.19). Consequently, an approximation to the daily insolation (all diffuse) for a ‘cloudy’ day can be estimated.

By assuming that the known average global insolation data can be represented by the sum of an appropriate number of ‘sunny’ days, estimated as described in Section 1.8.2.1 above with insolation given by (i), and ‘cloudy’ days with insolation given by (ii), the direct and diffuse components can then be

determined.

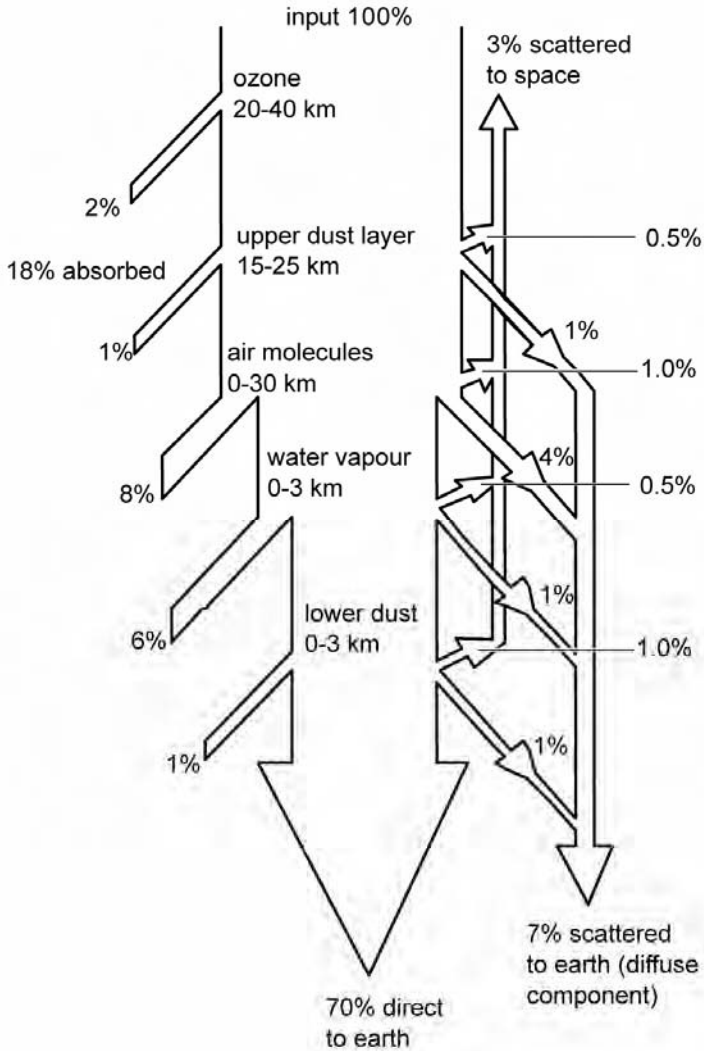


Figure 1.14. Typical AM1 clear sky absorption and scattering of incident sunlight (Used with permission of McGraw-Hill Companies, Hu, C. & White, R.M. (1983), Solar Cells: From Basic to Advanced Systems, McGraw-Hill, New York.).

As an aside, Eqn. (1.19) has been written independently of insolation wavelengths whereas, in reality, different wavelengths are attenuated to different degrees as empirically approximated by the expression (Hu & White, 1983)

$$I_{AMK}(\lambda) = I_{AM0}(\lambda) \left| \frac{I_{AM1}(\lambda)}{I_{AM0}(\lambda)} \right|^{AM^{0.678}} \quad (1.20)$$

where  $\lambda$  is the wavelength of light. Changes in spectral content can have a significant effect on the output of a solar cell. However, this effect is often neglected, since silicon solar cells absorb almost no light of wavelength greater than  $1.1 \mu\text{m}$  and module reflections increase at oblique angles of incident light, corresponding to longer wavelengths and increasing air mass.

### 1.8.4 Radiation on tilted surfaces

Since photovoltaic modules are commonly mounted at a fixed tilt, it is often necessary to estimate insolation on such tilted surfaces from that on the horizontal. This requires separate direct and diffuse components, as discussed above. Various models are available with a range of assumptions about the sky distribution of diffuse radiation (Duffie & Beckman, 1991; NASA, 2004a). Simple models are preferred if the input data is itself derived by modelling, such as, for example, from sunshine hours data (Perez *et al.*, 2001). Here, we consider only surfaces tilted towards the equator, although models are presented elsewhere for arbitrary orientations (Lorenzo, 1989).

#### Telecom method

Where insolation data is available in the form of direct and diffuse components, the following approach can be used to determine the corresponding insolation incident on a solar panel tilted at an angle  $\beta$  to the horizontal (after Mack, 1979).

First, we can assume the diffuse component  $D$  is independent of the tilt angle (which is a reasonably close approximation provided tilt angles are not much more than about  $45^\circ$ ). Lorenzo (2003) discusses several more comprehensive models considering, for example, the higher intensities close to the solar disk and near the horizon with clear skies.

Secondly, the direct component on the horizontal surface  $S$  is to be converted into the direct component  $S_\beta$  incident on a plane tilted at angle  $\beta$  to the horizontal as illustrated in Fig. 1.15.

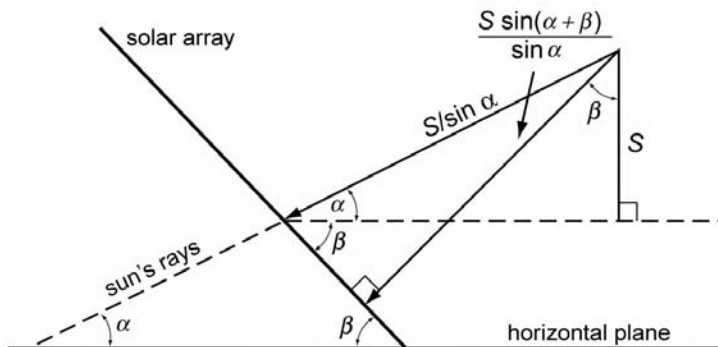


Figure 1.15. Light incident on a surface tilted to the horizontal (after Mack, 1979).

Consequently, we get

$$S_{\beta} = \frac{S \sin(\alpha + \beta)}{\sin \alpha} \quad (1.21)$$

where  $\alpha$  is the altitude of the sun (i.e. the angle between the sun and the horizontal) at noon, and is given by:

$$\alpha = 90^{\circ} - \theta - \delta \quad (1.22)$$

where  $\theta$  is the southern latitude.

The above is for solar modules facing north in the southern hemisphere. If facing south in the northern hemisphere, use  $\alpha = 90 - \theta + \delta$ , where  $\theta$  is, in this case, the northern latitude.

Eqn. (1.21) is only strictly correct at midday, although it is often used in system sizing to convert the direct component of mean daily solar radiation on a horizontal surface for solar panels at angle  $\beta$ , which introduces a small error.

Fig. 1.16 gives typical daily sunlight intensity profiles for a sunny and a cloudy winter's day. The cloudy day has a light intensity of only about 10% of that of the sunny day, owing to the boosting of the direct component relative to the diffuse component by tilting the array at  $60^{\circ}$  to the horizontal.

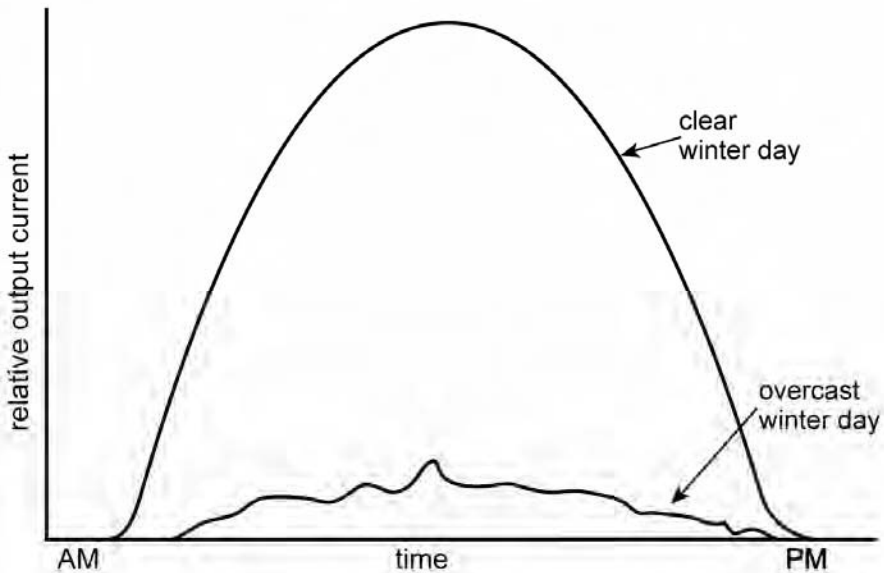


Figure 1.16. Relative output current from a photovoltaic array on a sunny and a cloudy winter's day in Melbourne ( $38^{\circ}\text{S}$ ) with an array tilt angle of  $60^{\circ}$  (after Mack, 1979).

Fig. 1.17 shows the effect of array tilting on the daily solar energy incidence for a location at latitude 23.5°N with a clear sky. Meinel and Meinel (1976, p. 108) tabulate the theoretical, clear sky daily energy interception for a range of fixed and tracking orientations at two representative latitudes for summer and winter solstices and the equinoxes.

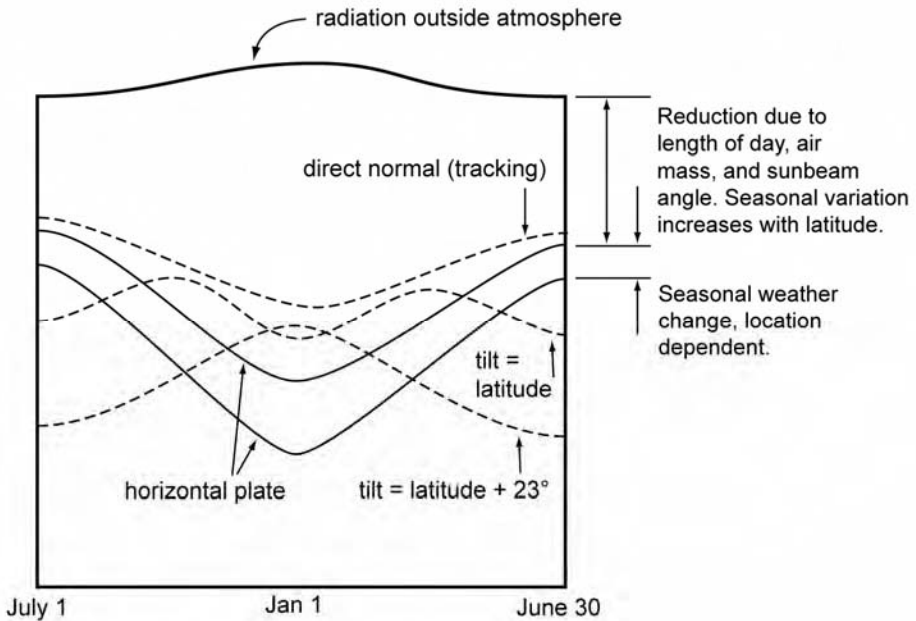


Figure 1.17. The effect of array tilting on the total insolation received each day for a location at latitude 23.4°N (Used with permission of McGraw-Hill Companies, Hu, C. & White, R.M. (1983), Solar Cells: From Basic to Advanced Systems, McGraw-Hill, New York.).

### Tilt towards equator

Lorenzo (2003) outlines the general method for converting monthly average daily radiation on the horizontal to monthly average daily radiation on an arbitrarily tilted surface. It requires estimation of hourly horizontal global, direct and diffuse components, their transposition to the tilted surface, and integration over a day. This procedure is computationally intensive and is done by some available PV system sizing computer programs.

However, as noted by Duffie and Beckman (1991, Section 2.19), a method has been devised by Liu and Jordan (1962) and extended by Klein (1977) for the special case of a flat surface tilted towards the horizon, for which a simple approximation may be used; that is

$$\bar{R}(\beta) = \bar{R}_b \left( 1 - \frac{\bar{R}_d}{\bar{R}} \right) + \bar{R}_d \frac{1 + \cos \beta}{2} + \bar{R} \frac{1 - \cos \beta}{2} \rho \quad (1.23)$$

where  $\rho$  is the ground reflectivity, the ratio  $\bar{R}_d / \bar{R}_o$  is correlated with  $\bar{K}_T$  as discussed in Section 1.8.3.1, and  $R_b$  is the ratio between the daily direct insolation on the tilted surface to that on the horizontal. The latter ratio is approximated by the same ratio of the corresponding extraterrestrial values. For the southern hemisphere, the ratio is given by

$$\bar{R}_b = \frac{\cos(\varphi + \beta) \cos \delta \sin \omega_{s,\beta}^* + \left(\frac{\pi}{180}\right) \omega_{s,\beta}^* \sin(\varphi + \beta) \sin \delta}{\cos \varphi \cos \delta \sin \omega_{s,\beta}^* + \left(\frac{\pi}{180}\right) \omega_{s,\beta}^* \sin \varphi \sin \delta} \quad (1.24a)$$

where

$$\omega_{s,\beta}^* = \min \left\{ \begin{array}{l} \cos^{-1}(-\tan \varphi \tan \delta) \\ \cos^{-1}(-\tan(\varphi + \beta) \tan \delta) \end{array} \right. \quad (1.24b)$$

is the sunset hour angle on the tilted surface for the characteristic day of the month. For the northern hemisphere

$$\bar{R}_b = \frac{\cos(\varphi - \beta) \cos \delta \sin \omega_{s,\beta}^* + \left(\frac{\pi}{180}\right) \omega_{s,\beta}^* \sin(\varphi - \beta) \sin \delta}{\cos \varphi \cos \delta \sin \omega_{s,\beta}^* + \left(\frac{\pi}{180}\right) \omega_{s,\beta}^* \sin \varphi \sin \delta} \quad (1.24c)$$

where

$$\omega_{s,\beta}^* = \min \left\{ \begin{array}{l} \cos^{-1}(-\tan \varphi \tan \delta) \\ \cos^{-1}(-\tan(\varphi - \beta) \tan \delta) \end{array} \right. \quad (1.24d)$$

Duffie and Beckman (1991) tabulate and plot values of  $\bar{R}_b$  for various tilt angles.

## 1.9 SOLAR ENERGY AND PHOTOVOLTAICS

Photovoltaics is inextricably linked with the development of quantum mechanics. Solar cells respond to light particles or *quanta*, although the wave-particle duality of light cannot be overlooked in cell design.

Sunlight itself approximates ideal blackbody radiation outside the earth's atmosphere. The inability to explain such blackbody radiation by classical theory was itself responsible for the development of quantum mechanics, which in turn was needed to understand solar cell operation. As well as reflecting light from the sun, the earth itself emits radiation similar to that of a blackbody, but centred at much greater wavelengths because of its lower temperature.

Absorption and scattering of light by the earth's atmosphere reduce the intensity and wavelength distribution of light reaching the earth's surface. They also interfere with energy being radiated by the earth, resulting in higher terrestrial temperatures than on the moon and a sensitivity of terrestrial temperature to 'anthropogenic' greenhouse gases. Owing to the variability of the intensity and wavelength distribution of

terrestrial light, a standard solar spectrum is used to rate photovoltaic products. The present standard for most terrestrial applications is the global Air Mass 1.5 spectrum tabulated in Appendix A.

## EXERCISES

- 1.1 The sun is at an altitude of  $30^\circ$  to the horizontal. What is the corresponding air mass?
- 1.2 What is the length of the shadow cast by a vertical post with a height of 1 m under AM1.5 illumination?
- 1.3 Calculate the sun's altitude at solar noon on 21 June in Sydney (latitude  $34^\circ\text{S}$ ) and in San Francisco (latitude  $38^\circ\text{N}$ ).
- 1.4 The direct radiation falling on a surface normal to the sun's direction is  $90 \text{ mW/cm}^2$  at solar noon on one summer solstice in Albuquerque, New Mexico (latitude  $35^\circ\text{N}$ ). Calculate the direct radiation falling on a surface facing south at an angle of  $40^\circ$  to the horizontal.
- 1.5 To design appropriate photovoltaic systems, good data on the insolation (i.e. amount of sunshine) is essential for each particular location. List the sources and nature of insolation data available for your region (state or country).

## REFERENCES

*Updated World Wide Web links can be found at [www.pv.unsw.edu.au/apv\\_book\\_refs](http://www.pv.unsw.edu.au/apv_book_refs).*

ASTM (2000), 'Standard solar constant and air mass zero solar spectral irradiance tables', Standard No. E 490-00.

ASTM (2003), *G173-03 Standard Tables for Reference Solar Spectral Irradiances: Direct Normal and Hemispherical on  $37^\circ$  Tilted Surface* ([www.astm.org](http://www.astm.org)).

Australian Bureau of Meteorology (2004) ([www.bom.gov.au/weather/satellite](http://www.bom.gov.au/weather/satellite)).

Beyer, H.G., Reise, C. & Wald, L. (1992), 'Utilization of satellite data for the assessment of large scale PV grid integration', Proc. 11th EC Photovoltaic Solar Energy Conference, Montreux, Switzerland, pp. 1309–1312.

Blakers, A., Green, M., Leo, T., Outhred, H. & Robins, B. (1991), *The Role of Photovoltaics in Reducing Greenhouse Gas Emissions*, Australian Government Publishing Service, Canberra.

Bureau of Meteorology (1991), Australia.

Duffie, J.A. & Beckman, W.A. (1991), *Solar Engineering of Thermal Processes*, 2nd Edition, Wiley-Interscience, New York.

Gast. P.R., (1960), 'Solar radiation', in Campen *et al.*, *Handbook of Geophysics*, McMillan, New York, pp. 14-16–16-30.

- Glover, J. & McCulloch, J.S.G. (1958), *Quarterly Journal of the Royal Meteorological Society*, **84**, pp. 172–175.
- Gribben, J. (1984), *In Search of Schrödinger's Cat*, Corgi Books, Transworld Publishers, London.
- Gueymard, C.A. (2004), 'The sun's total and spectral irradiance for solar energy applications and solar radiation models', *Solar Energy*, **76**, pp. 423–453.
- Hall, I.J., Prairie, R.R., Anderson, H.E., Boes, E.C. (1978), 'Generation of a typical meteorological year', Proc. 1978 annual Meeting of the American Section of the International Solar Energy Society, Denver, **2**, p. 669.
- Hu, C. & White, R.M. (1983), *Solar Cells: From Basic to Advanced Systems*, McGraw-Hill, New York.
- Incropera, F.P. and DeWitt, D.P. (2002), *Fundamentals of Heat and Mass Transfer*, 5th Edn., Wiley, New York.
- Iqbal, M. (1983), *An Introduction to Solar Radiation*, Academic, Toronto.
- Klein, S.A. (1977), 'Calculation of monthly-average insolation on tilted surfaces', *Solar Energy*, **19**, p. 325.
- Lee, T., Oppenheim, D. & Williamson, T. (2003), *Australian Solar Radiation Handbook (AUSOLRAD)*, Australian and New Zealand Solar Energy Society, Sydney ([www.anzsos.org/Bookshop/Asr.html](http://www.anzsos.org/Bookshop/Asr.html)).
- Liu, B.Y. & Jordan, R.C. (1960), 'The inter-relationship and characteristic distribution of direct, diffuse and total solar radiation', *Solar Energy*, **4**, pp. 1–19.
- Liu, B.Y. & Jordan, R.C. (1962), 'Daily insolation on surfaces tilted toward the equator', *ASHRAE Journal*, **3**, p. 53.
- Lorenzo, E. (1989), 'Solar radiation', in Luque, A. (Ed.), *Solar Cells and Optics for Photovoltaic Concentration*, Adam Hilger, Boston and Philadelphia, pp. 268–304.
- Lorenzo, E. (2003), 'Energy collected and delivered by PV modules', in Luque, A. & Hegedus, S. (Eds.), *Handbook of Photovoltaic Science and Engineering*, Wiley, Chichester, pp. 905–970.
- Mack, M. (1979), 'Solar power for telecommunications', *The Telecommunication Journal of Australia*, **29**(1), pp. 20–44.
- McCarthy, J., Canziani, O.F., Leary, N.A., Dokken, D.J. & White, K.S. (Eds.) (2001), *Climate Change 2001: Impacts, Adaptation, and Vulnerability*, Contribution of Working Group II to the Third Assessment Report of the Intergovernmental Panel on Climate Change, Geneva.
- Meinel, A.B. & Meinel, M.P. (1976), *Applied Solar Energy: An Introduction*, Addison Wesley Publishing, Reading.
- Muirhead, I.J. & Kuhn, D.J. (1990), 'Photovoltaic power system design using available meteorological data', Proc. 4th International Photovoltaic Science and Engineering Conference, Sydney, 1989, pp. 947–953.

- NASA (2004a), 'Surface meteorology and solar energy' (eosweb.larc.nasa.gov/sse).
- NASA (2004b), 'NASA surface meteorology and solar energy: methodology' (eosweb.larc.nasa.gov/cgi-bin/sse/sse.cgi?na+s08#s08).
- NIST (2002), *CODATA Internationally recommended values of the fundamental physical values*, National Institute of Standards and Technology (physics.nist.gov/cuu/Constants).
- NREL (2005), *US Solar Radiation Resource Maps*, (rredc.nrel.gov/solar/old\_data/nsrdb/redbook/atlas).
- Page, J. (1961), 'The estimation of monthly mean values of daily total short-wave radiation on vertical and inclined surfaces from sunshine records for latitudes 40°N–40°S', UN Conference on New Energy Sources, paper no. S98, 4, pp. 378–390.
- Perez, R., Aguiar, R., Collares-Pereira, M., Diumartier, D., Estrada-Cajigal, V., Gueymard, C., Ineichen, P., Littlefair, P., Lüne, H., Michalsky, J., Olseth, J.A., Renne, D., Rymes, M., Startveit, A., Vignola, F. & Zelenka, A. (2001), 'Solar resource assessment: A review', in Gordon, J. (Ed.), *Solar Energy: The State of the Art*, James & James, London.
- Quaschnig, V. & Hanitsch, R. (1995), 'Quick determination of irradiance reduction caused by shading at PV-locations', Proc. 13th European Photovoltaic Solar Energy Conference, pp. 683–686.
- Quaschnig, V. (2003), 'Technology fundamentals: The sun as an energy resource', *Renewable Energy World*, 6(5), pp. 90–93.
- Reddy, T.A. (1987), *The Design and Sizing of Active Solar Thermal Systems*, Oxford University Press, Chapter 4.
- Reitveld, M.R. (1978), 'A new method for estimating the regression coefficients in the formula relating solar radiation to sunshine', *Agricultural Meteorology*, 19, pp. 243–252.
- Sandia National Laboratories (1991), *Stand-Alone Photovoltaic Systems. A Handbook of Recommended Design Practices* (SAND87-7023) (www.sandia.gov/pv/docs/Programmatic.htm).
- Skiba, M., Faller, F.R., Eikmeier, B., Ziolek, A. and Unge, H. (2000), 'Skiameter shading analysis', Proc. 16th European Photovoltaic Solar Energy Conference, James & James, Glasgow, pp. 2402–2405.
- Sproul, A. B. (2002), 'Vector analysis of solar geometry', Proc. Solar 2002, Conference of the Australian and New Zealand Solar Energy Society, Newcastle.
- Standards Australia (2002), *Stand-Alone Power Systems. Part 2: System Design Guidelines*, AS 4509.2.
- Twidell, J. & Weir, T. (2006), *Renewable Energy Resources*, 2nd Edn., Taylor and Francis, Abingdon and New York.

University of Oregon (2003), 'Sun chart program, University of Oregon Solar Radiation Monitoring Laboratory' ([solardat.uoregon.edu/SunChartProgram.html](http://solardat.uoregon.edu/SunChartProgram.html)).

Willson, R.C. & Hudson, H.S. (1988), 'Solar luminosity variations in solar cycle 21', *Nature*, **332**, pp. 810–812.